

RESEARCH ARTICLE

Efferocytosis and extrusion of leukocytes determine the progression of early mycobacterial pathogenesis

Rohola Hosseini, Gerda E. M. Lamers, Hiwa M. Soltani, Annemarie H. Meijer, Herman P. Spaink and Marcel J. M. Schaaf[‡]

ABSTRACT

Macrophages and neutrophils are the first responders to invading pathogens and contribute strongly to the host defense against intracellular pathogens. The collective interplay and dynamic interactions between these leukocytes are to a large extent not understood. In the present study, we have investigated their role using a combination of confocal laser-scanning and electron microscopy in a zebrafish model for tuberculosis, a local *Mycobacterium marinum* infection in the tissue of the larval tail fin. Our results show that neutrophils are efficient in phagocytosis of mycobacteria and that they contribute largely to their dissemination. Macrophages appear to play a major role in efferocytosis, phagocytosis of dead cells that contain bacterial content. Phagocytic cells with large bacterial aggregates are formed that can be extruded out of the tissue after cell death. Alternatively, these excessively infected cells can undergo necrosis leading to immediate recruitment of surrounding leukocytes and subsequent phagocytosis of released bacteria. Our data show that these necrotic burst events result in progression of the infection, whereas extrusion abates the infection.

KEY WORDS: Zebrafish, Tail fin, Infection, *Mycobacterium*, Microscopy, Macrophage, Neutrophil, Leukocyte dynamics, Extrusion, Efferocytosis, Cell death

INTRODUCTION

In humans, pulmonary tuberculosis (TB) is a bacterial infection caused by *Mycobacterium tuberculosis* (*Mtb*). Upon infection often no symptoms are observed, and this condition is known as latent tuberculosis. It is estimated that one third of the world population has a latent TB infection, that progresses to active TB in 5–10% of cases. TB has been responsible for a high mortality in human populations and is still a major health issue. Worldwide, new cases of TB are diagnosed every second and one TB patient does not survive the infection every 20 s (WHO, 2015: <http://www.who.int/tb/publications/en/>).

To study the disease and host–pathogen interactions during mycobacterial infection, the zebrafish model for TB has been an effective approach (Davis et al., 2002; Tobin et al., 2010; Cambier et al., 2014; van der Vaart et al., 2014). The zebrafish, and other fish and frog species, are naturally susceptible to a mycobacterial disease, caused by *Mycobacterium marinum* (*Mm*), which is genetically related to *Mtb*. The disease shows a similar pathogenesis to its human equivalent, including the formation of


granulomatous lesions (Davis et al., 2002; Swaim et al., 2006). The high level of similarity between the zebrafish and human immune system, which consist of comparable cell types, makes the zebrafish a suitable animal model to study host–pathogen interactions (Renshaw and Trede, 2012). The presence of macrophages and neutrophils during the larval stage has been demonstrated, and these cells have been shown to be the first responders to invading pathogens. During the early stages of TB infection they are the main cell types to be infected (Silva et al., 1989; Eum et al., 2010), and macrophages have been demonstrated to be sufficient for the formation of early granuloma structures during *Mm* infection (Davis et al., 2002). In contrast, cells of the adaptive immune system do not mature during the first 2 weeks of development.

Mycobacteria ingested by macrophages are encapsulated in phagosomes and, upon ingestion, these cells activate an array of intracellular effector mechanisms. These mechanisms are aimed at the elimination of bacteria inside the phagosomes or the fusion of the phagosomes with lysosomes, and include acidification of compartments, and production of oxidants, nitrosylating agents, antimicrobials and proteases (MacMicking, 2012; Torraca et al., 2014). Recent studies have demonstrated additional mechanisms restricting mycobacterial proliferation including efferocytosis, which is the phagocytosis of dead cells containing pathogens (Weiss and Schaible, 2015). In response to the capability of host cells to eliminate them, pathogenic mycobacteria have evolved mechanisms for the manipulation of the host immune response by secretion of virulence factors through specialized secretion systems (Baxt et al., 2013; Houben et al., 2013). The bacteria are able to prevent lysosomal fusion and acidification of phagosomal compartments (Armstrong and Hart, 1971; Tan and Russell, 2015). Although a fraction of *Mtb* within a host cell is kept inside phagosomes, another fraction is able to escape from the phagosomes into the cytoplasm (van der Wel et al., 2007; Simeone et al., 2015).

Although macrophages are the main cell type commonly associated with mycobacterial infection, a growing body of evidence is showing that other phagocytic cells also play a major role during mycobacterial infection (Berry et al., 2010; Lowe et al., 2012; Nouailles et al., 2014; Srivastava et al., 2014). In the lungs of animals infected with *Mtb*, several cell types are found to be recruited and to contain bacteria. Besides alveolar macrophages, neutrophils, monocytes, interstitial macrophages and dendritic cells are found to be recruited to the infected lungs in response to inflammatory signals (Srivastava et al., 2014). Neutrophils in particular, appear to play a crucial role during a mycobacterial infection and are often the first responders in the host defense towards invading pathogens, (Silva et al., 1989; Lowe et al., 2012). Neutrophils are less studied than other cell types involved in the host response towards mycobacterial infections. In the zebrafish model, neutrophils are observed to have a direct interaction with

Institute of Biology Leiden, Leiden University, Leiden 2333CC, The Netherlands.

[‡]Author for correspondence (m.j.m.schaaf@biology.leidenuniv.nl)

 H.P.S., 0000-0003-4128-9501; M.J.M.S., 0000-0002-5859-8936

Received 15 February 2016; Accepted 25 July 2016

mycobacteria (Meijer et al., 2007), and inhibition of neutrophil recruitment to the infection site results in an enhanced mycobacterial burden (Yang et al., 2012). Neutrophils have been shown to become infected upon recruitment to established granulomas and are able to actively eliminate the mycobacteria by means of oxidative mechanisms (Yang et al., 2012). Enhanced production of reactive nitrogen species (RNS) by neutrophils through the transcription factor hypoxia-inducible factor 1- α (Hif-1 α) plays an important role in mycobacterial elimination (Elks et al., 2013). These results show that innate immune cell types other than macrophages also contribute to host defense against mycobacterial infections.

The balanced interplay between macrophages and neutrophils and their specific dynamic interactions during the host response against intracellular pathogens are still unclear. The present study focuses on the quantification and high-resolution imaging of macrophage and neutrophil function and dynamics during mycobacterial infection. This is required to obtain a better understanding of the specific role that infected macrophages and neutrophils play during infection and their collective contribution to the host defense and bacterial dissemination. We have investigated the complex dynamic response of macrophages and neutrophils towards mycobacterial infection using *Mm*. We have utilized the previously described zebrafish tail fin infection model (Hosseini et al., 2014), which enables us to visualize the entire infection process using time-lapse confocal laser scanning microscopy (CLSM) in combination with advanced 3D block-face scanning electron microscopy (SBFSEM). Our results show that neutrophils are able to phagocytose mycobacteria and contribute to their dissemination. Macrophages play a major role in efferocytosis of dead infected leukocytes resulting in large bacterial aggregates inside these cells. Subsequently, these highly infected macrophages can undergo necrosis with a burst-like response, spreading the mycobacteria to freshly attracted macrophages and neutrophils. Finally, extrusion of dead cells containing bacteria out of the host tissue appears to effectively decrease the bacterial burden.

RESULTS

Zebrafish larvae were infected with ~50 colony-forming units (cfu) *Mm* in the tail fin at 3 days post fertilization (dpf). We used larvae from a transgenic line, *Tg(mpeg1:eGFP) X Tg(lyz:DsRed2)*, which displays green and red fluorescent macrophages and neutrophils, respectively (Ellett et al., 2011; Hall et al., 2007). Injection of *Mm* in the tail fin induces a localized infection, which attracts macrophages and neutrophils to the site of infection, and develops into a granuloma-like structure within 5 days post infection (dpi) (Fig. 1A; Hosseini et al., 2014). At this early stage of development, the zebrafish tail fin consists of two epithelial cell layers on both sides, with mesenchyme cells in between, and no leukocytes are normally found there (Kimmel et al., 1995). In order to provide a detailed description of the infection process and the host response, time-lapse imaging using confocal laser scanning microscopy (CLSM) was performed.

The bacterial burden and the number of macrophages and neutrophils recruited to the site of infection was quantified at 1, 6 and 12 h post infection (hpi) and at 1, 2, 3, 4 and 5 dpi (Fig. 1B–D). Representative images for these time points are shown in Fig. 1B. The bacterial burden did not change between 1 hpi and 1 dpi, but increased significantly between 1 and 3 dpi after which it remained unchanged until 5 dpi (Fig. 1C). Upon infection, the number of recruited macrophages remains constant (at approximately 3) until 1 dpi, whereas the number of neutrophils

decreased significantly from 4.2 (\pm 0.3) at 1 hpi to 1.1 (\pm 0.3) at 12 hpi (mean \pm s.e.m.; Fig. 1C). At this time point, the macrophages were the main type of leukocyte present at the site of infection and the majority of these macrophages (~72%) were infected with *Mm*. After this time point, both the number of macrophages and neutrophils increased dramatically and they remained constant after 4 dpi (Fig. 1C). Based on the bacterial burden at the site of infection, three different phases of the mycobacterial infection can be distinguished, the lag, exponential and stationary phase (Fig. 1E).

To investigate the lag phase of infection, image sequences acquired using time-lapse microscopy were analyzed in detail focusing on leukocyte dynamics and cell death (Fig. 2; Movie 1). Fig. 2A shows representative images taken at different time points during the lag phase of infection. These images show that during this lag phase the bacterial burden remained constant and the number of macrophages also remained constant. However, the number of neutrophils decreased steadily, due to the reverse migration and the short lifespan of infected neutrophils.

Reverse migration of infected neutrophils during the lag phase

Using these image sequences, the trajectories of the macrophages and neutrophils were analyzed (until the moment they had moved out of the field of view or had undergone cell death). Infected macrophages and neutrophils showed short trajectories and the vast majority of these cells (~84%) stayed within the tail fin (Fig. 2B,C). A fraction of infected macrophages (9 \pm 5%, mean \pm s.e.m.) and neutrophils (28 \pm 8%) was observed to migrate away from the infection site (Fig. 2B; infected N2). Generally, these leukocytes migrated along the caudal vein (marked in Fig. 2B as infected N2) and were not observed to intravasate the caudal vein. Uninfected macrophages showed short trajectories towards and away from the infection site, whereas uninfected neutrophils showed longer trajectories covering a large area of the tail fin (Fig. 2D). It has previously been shown that the macrophage versus neutrophil fate can be manipulated in zebrafish embryos by *irf8* knockdown, which increases neutrophil numbers at the expense of macrophages (Li et al., 2011). Upon depletion of macrophages using an *irf8* morpholino the number of bacterial clusters was counted outside the region of interest, as indicated in Fig. 2A (Fig. S1). The *irf8* morphants showed a higher number of bacterial clusters outside the ROI compared to control larvae, on average 2.3 \pm 0.4 and 1.0 \pm 0.4, respectively. These data confirm our time-lapse imaging, and indicate that neutrophils have a large contribution to the dissemination of the bacteria.

The lifespan of infected leukocytes is dependent on the bacterial burden

The acquired image sequences were additionally used to determine the lifespan of neutrophils and macrophages after infection. The lifespan for each cell was based on the time from the initial phagocytosis of bacteria until the moment of cell death. Infected macrophages have an average lifespan of 4.8 h (\pm 0.5) compared to 3.1 h (\pm 0.6, mean \pm s.e.m.) for neutrophils. The bacterial content of these cells correlated with their lifespan (Spearman correlation coefficient -0.52 , $P < 0.0001$); the higher the bacterial content, the shorter their lifespan (Fig. 2E,F). For the population of macrophages, the distribution of individual lifespans showed a continuum (Fig. 2E), whereas for neutrophils we found a bimodal distribution. The majority of infected neutrophils had a very short lifespan (<1 h), and showed a bacterial content larger than ~50 μm^2 (in a 2D image). Neutrophils with a smaller bacterial content had a

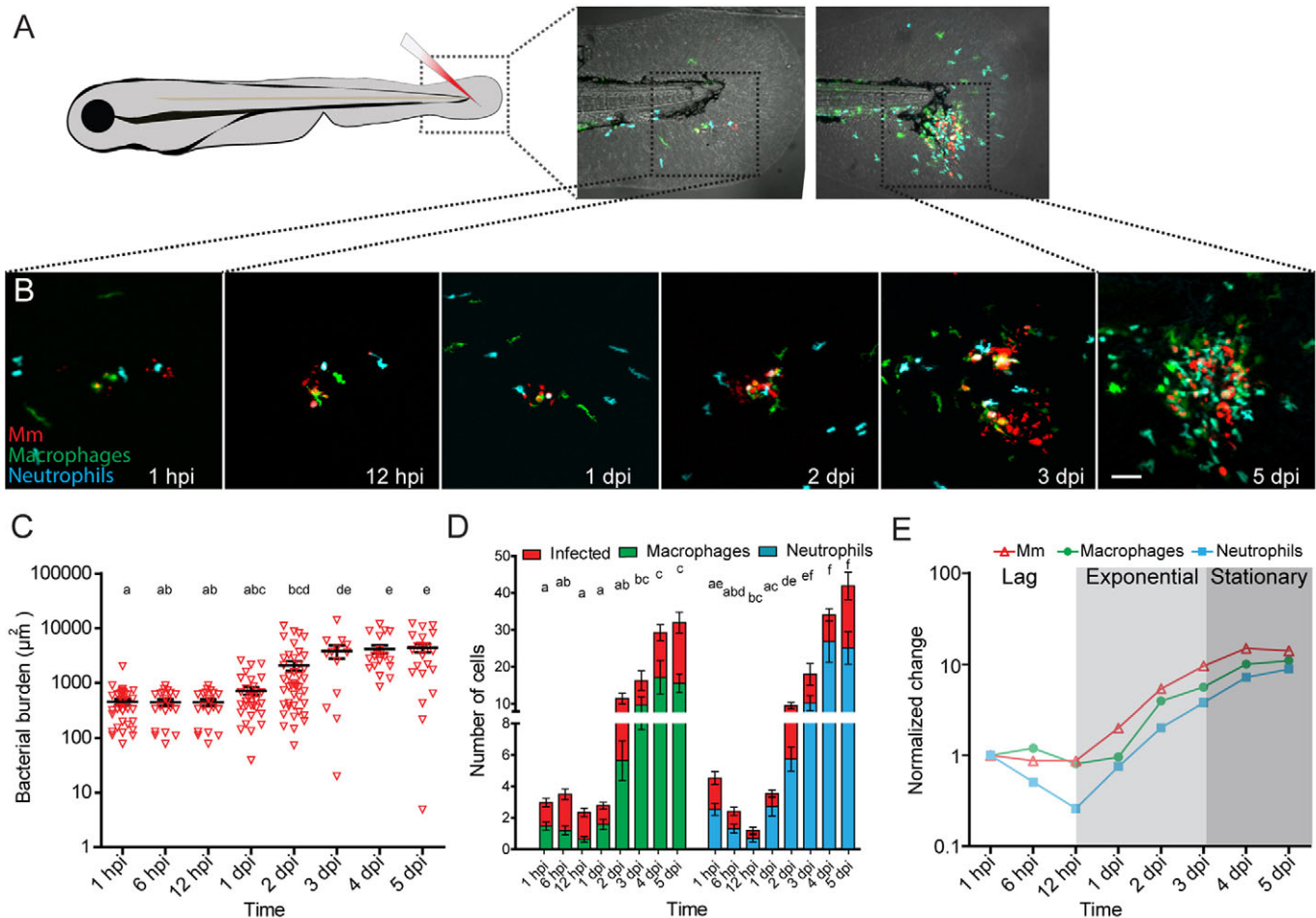


Fig. 1. *Mm* infection in the zebrafish tail fin. (A) Schematic image showing the location in the tail fin where *Mm* was injected into zebrafish larvae at 3 dpf. (B) Representative CLSM images of the infection site in the tail fin at different time points. (C) Quantification of the bacterial burden at different time points after *Mm* infection. (D) Numbers of macrophages (green) and neutrophils (blue) recruited to the site of infection and their infected fractions (red) per larva. (E) Normalized bacterial burden and numbers of recruited leukocytes (relative to 1 hpi). The analysis shows that based on the bacterial burden, the course of infection can be divided into three different phases: the lag, exponential and stationary phase. Error bars indicate s.e.m. ($n \sim 20$ larvae per time point); means with the same letter do not differ significantly (Dunnett's post-test, $P < 0.05$). Scale bar: 50 μm .

longer lifespan, 0–15 h compared to 0–3 h for larger bacterial content (Fig. 2F).

Different morphologies of cell death

We found that infected leukocytes underwent cell death, which is defined here as a disappearance of the fluorescent signal. We could distinguish three specific, not mutually exclusive, patterns for leukocytes undergoing cell death. The quantification of these different patterns was based on the morphological features of 45 infected macrophages and 41 infected neutrophils that were fluorescently labeled. They were followed for up to 18 h using CLSM (Fig. 2G). Representative examples of macrophages and neutrophils showing these morphological features are presented in Fig. S2. The majority of leukocytes undergoing cell death displayed a fragmentation of the cell into several compartments, of which at least one contained bacteria. The fluorescent signal of these compartments disappeared after different time intervals, ranging from a few minutes to several hours (see also Movies 2 and 3). Approximately 33% of macrophages and 24% of neutrophils displayed this form of cell death. The second cell-death-associated pattern that we observed was a round morphology before the disappearance of the signal (in 13% macrophages and 30%

neutrophils). The time between rounding up of the cell and disappearance of the signal varied from a few minutes to several hours (see also Movies 2 and 4). The third pattern of cell death was characterized by a rapid signal disappearance. In these leukocytes, the fluorescent signal disappeared within a few minutes after phagocytosis of bacteria (Fig. S2C,D). Additional examples of macrophage and neutrophil showing rapid signal disappearance are presented in Movies 1 and 5. Approximately 30% of macrophages and 16% of neutrophils displayed this pattern of cell death. The cells showing multiple patterns were assigned to the multiple group.

Efferocytosis of dead cells by macrophages

Regardless of the pattern of cell death of infected leukocytes, secondary uptake of the bacterial content by macrophages was observed in most cases (Fig. 2H). This secondary uptake most likely includes phagocytosis of the dying or dead cells, which is called efferocytosis (Martin et al., 2013). The secondary uptake of bacterial content that had initially been sequestered by macrophages or neutrophils was performed by macrophages in $\sim 85\%$ of the cases (Fig. 2H). In the remaining $\sim 15\%$ of the cases, this efferocytosis was carried out by neutrophils. In Fig. 2I

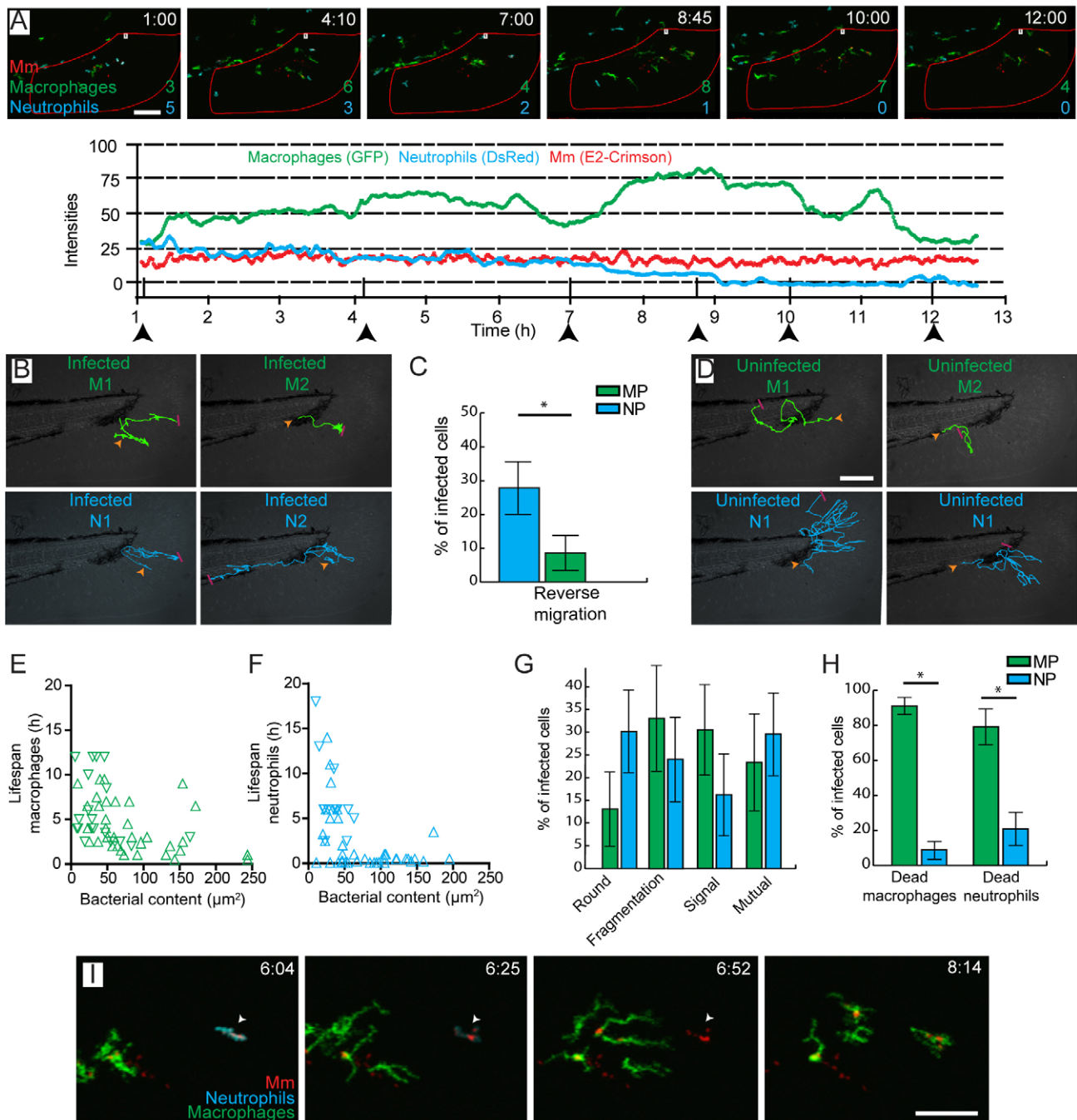


Fig. 2. Accumulation of *Mm* in macrophages occurs through cell death and secondary uptake by macrophages at the site of infection. (A) Intensity profiles for macrophages (green), neutrophils (blue) and *Mm* (red) at the site of infection in a representative larva, showing dynamic recruitment and resolution of leukocytes. Corresponding images are shown for the time points indicated by the arrowheads, in which the numbers of leukocytes present within the region of interest (red outline) are indicated. (B) Representative trajectories of infected leukocytes. Macrophage 1 (M1) and neutrophil 1 (N1) show short local trajectories in the tail fin. Macrophage 2 (M2) was recruited to the site of infection and remains at the same position after phagocytosis of *Mm*. Neutrophil 2 (N2) shows reverse migration along the caudal vein. (C) Percentages of leukocytes per larva showing reverse migration. MP, macrophages; NP, neutrophils. (D) Representative trajectories of uninfected macrophages (green) and neutrophils (blue). The macrophages show short trajectories into and out of the tail fin, whereas the neutrophils show longer trajectories in the tail fin before going out. (E, F) Lifespan of infected leukocytes as a function of the infection size at the lag phase of infection. (G) Percentages of infected leukocytes undergoing cell death showing different morphologies. (H) Phagocytosis by macrophages and neutrophils of the bacterial content of leukocytes that have undergone cell death. (I) Representative frames from time-lapse imaging showing phagocytosis by a macrophage of bacterial content, which was initially sequestered inside a neutrophil (arrowhead). In B and D, the orange arrowhead represents the start and the red bar represents the end of the trajectory. Error bars indicate s.e.m. ($n \sim 20$ larvae per time point). * $P < 0.05$ (Mann–Whitney test). Scale bars: 50 μm .

(Movie 1) an example is shown of efferocytosis by a macrophage taking up an infected neutrophil that has undergone cell death as shown by the rapid disappearance of the fluorescent signal.

At the beginning of the exponential phase (12 hpi), the bacterial infection was mainly present in macrophages due to the continuous neutrophilic cell death and efferocytosis during the lag phase. In

order to study the progression of the infection from 12 hpi to 2 dpi, we analyzed time-lapse recordings of this period. Two events are characteristic for this phase of the infection process: macrophage burst and extrusion of bacteria (Fig. 3).

Macrophage burst events

In our study, macrophage burst events were defined as highly infected macrophages undergoing necrotic cell death, probably due to cell-death-induced rupture of the membranes surrounding these cells, and spreading of the bacteria to freshly recruited leukocytes (Repasy et al., 2013). Subsequently, the spread bacteria were taken

up by neutrophils and macrophages. An example of such a burst event imaged using time-lapse CLSM is shown in Fig. 3A and Movie 6. The number of burst events increased dramatically between 1 and 3 dpi, from 0.1 (± 0.08) to 2.4 (± 1.1 , mean \pm s.e.m.) burst events per larva. This is probably due to the increased bacterial burden per cell.

Extrusion of *Mm* aggregates

Interestingly, large aggregates of bacteria were also observed to be extruded out of the tail fin. The frequency of these extrusion events significantly increased between 1 and 3 dpi, from 0.8 (± 0.1) to 6.9

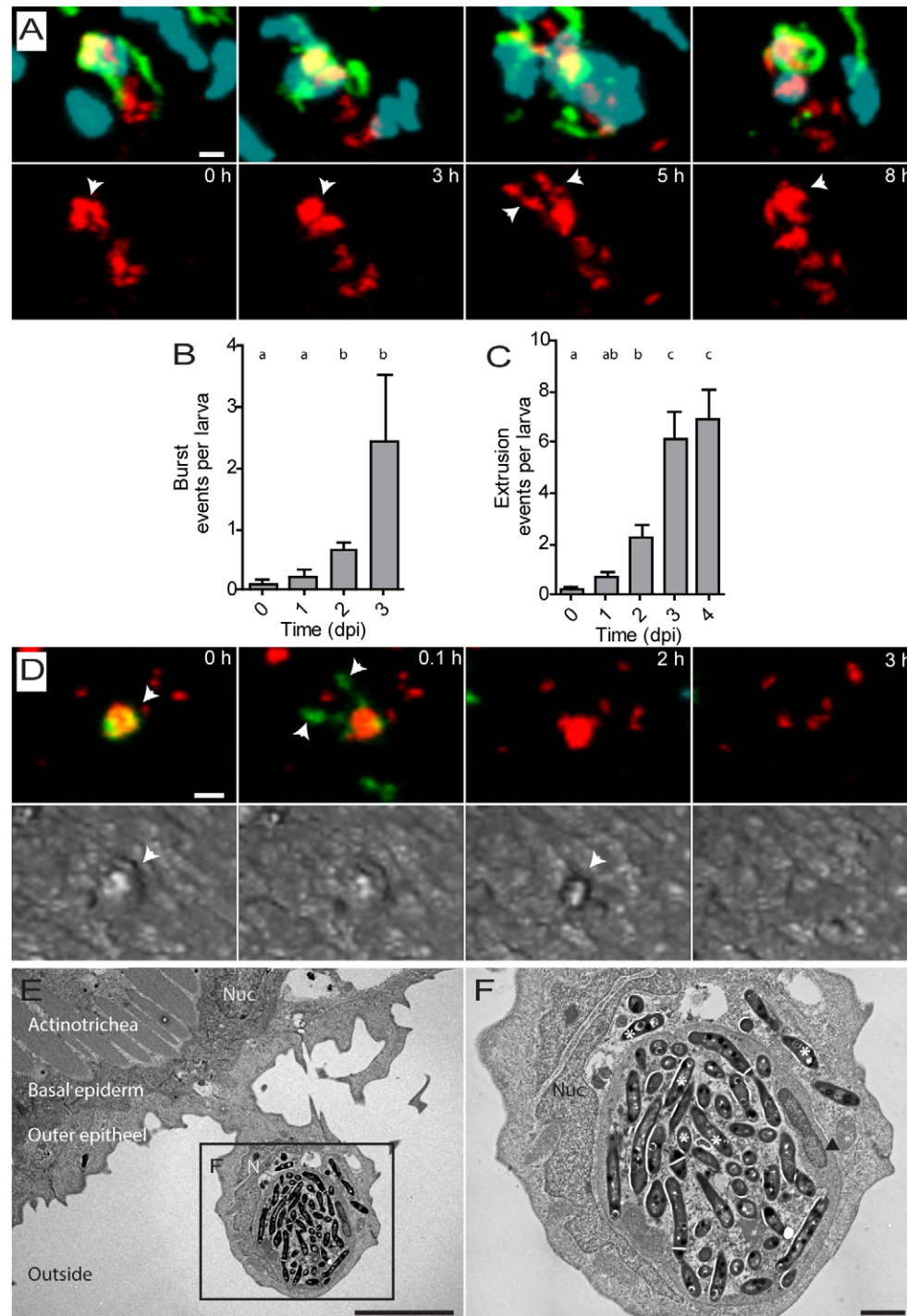


Fig. 3. Macrophages containing aggregates of *Mm* undergo burst or extrusion. (A) Representative images from live-cell imaging of a large aggregate of *Mm* (arrowhead) inside a macrophage undergoing cell death at $t=3$ h. Spreading of *Mm* was observed at $t=5$ h. The aggregate was compacted again by newly recruited leukocytes at $t=8$ h (see Movie 6). (B) Number of burst events observed at different time points after *Mm* infection in the tail fin. (C) Number of extrusion events observed at different time points after *Mm* infection in the tail fin. (D) Representative images from live-cell imaging showing an extrusion event for accumulated *Mm* in a macrophage (arrowheads). First, the macrophage undergoes cell death and subsequently after 3 h the bacterial content is extruded. (E) TEM image of an extruding epithelial cell from the tail fin surrounding a dead cell containing a large aggregate of *Mm*. The two epithelial layers and actinotrichia are indicated. (F) Higher magnification of the region indicated in E, showing compact aggregates of *Mm* (asterisks) in the dead cell with a condensed nucleus (arrowhead). Error bars indicate s.e.m. ($n \sim 20$ larvae per time point), means with the same letter do not differ significantly (Dunnnett's post-test, $P < 0.05$). Scale bars: 10 μ m (A,D,E); 2 μ m (F).

(± 1.1) extrusion events per larva (mean \pm s.e.m., Fig. 3C). An example of an extrusion event imaged using time-lapse CLSM is shown in Fig. 3D and Movie 7. As in most cases, in this example the bacterial content was initially present in a macrophage, and was extruded 2 to 3 h after disappearance of the fluorescent signal of the macrophage. These extrusion events were not exclusively observed upon cell death of macrophages, but also occurred occasionally after neutrophil cell death. The extruded bacterial aggregate could be first visualized as a protuberance on the outer epithelial layer of the tail fin, which could be observed using brightfield (differential interference contrast) microscopy (Fig. 3D). The ultrastructure of such a protuberance in another larvae was imaged using transmission electron microscopy (TEM). These images show a bacterial aggregate shortly before an extrusion event (Fig. 3E). A cell of the outer epithelial layer containing a dead cell with a large bacterial aggregate (Fig. 3F), is in the process of being extruded from the epithelial layer. The light microscopy data show that bacterial aggregates are extruded from the tissue. However, the electron microscopy images of this process demonstrate that the aggregate is located within a dead leukocyte, which has been phagocytized by the epithelial cell.

The stationary phase of infection is characterized by granuloma-like structures containing a large number of macrophages and neutrophils at the site of infection. In this phase, we observed secondary granuloma-like structures (Fig. S3), which are most often observed near the caudal vein. Additionally, at this phase, extrusion occurred at a large scale and the bacterial contents of several cells were observed to be simultaneously extruded.

Ultrastructure of infected macrophages and neutrophils

In order to get a deeper understanding of cellular processes ongoing in the infected leukocytes, infected larvae were analyzed using electron microscopy. We used 3D serial block-face SEM (SBFSEM) to obtain a 3D electron microscopy image of the region of the infected tail fin at 3 dpi (Movie 8). In this technique, electron microscopy images are acquired from the surface of the tissue sample. Subsequently, a 100 nm layer is removed and a new image of the surface is acquired (Denk and Horstmann, 2004; Peddie and Collinson, 2014). To correlate these 3D SEM images with images obtained by CLSM, the bacteria observed in the SBFSEM images were aligned with the fluorescent signal of *Mm* acquired by CLSM (Fig. S4). By aligning the images acquired by the two techniques, the fluorescently labeled macrophages and neutrophils were identified in the SBFSEM images (Fig. 4A,B). Using this approach the SBFSEM images of the infected macrophages and neutrophils could not only be correlated with the CLSM images, but could also be linked to the dynamic behavior of these cells, as observed by CLSM in the previous hours (Movie 9).

The images of two infected macrophages and two infected neutrophils were correlated (indicated in Fig. 4A,B). The electron microscopy image of the first macrophage (M1) showed clear chromatin condensation in the nucleus, which was not observed in other macrophages within same sample (Fig. 4C). The CLSM images showed that this cell had phagocytized a large aggregate of bacteria ~ 30 min earlier (Fig. 4D). The second imaged macrophage (M2) showed a single compartment containing a bacterial aggregate and remains of dead cells in the electron microscopy images (Fig. 4C). The CLSM images show that this macrophage had phagocytized the aggregate ~ 1.5 h earlier (Fig. 4D) and no sign of cell death was apparent in the electron microscopy image (Fig. 4C).

The first imaged neutrophil (N1) displays a necrotic morphology in the electron microscopy images, characterized by a round nucleus

and an irregularly shaped plasma membrane and no apoptotic features (Fink and Cookson, 2005). In the CLSM images, this neutrophil shows a compacted bacterial content at the start of the time lapse and a disappearance of the fluorescent signal (within 1 min) at ~ 30 min before the end of the time lapse (the time point of fixation) (Fig. 4C). Based on our correlated light and electron microscopy images, we suggest that the type of cell death characterized by a rapid disappearance of the fluorescent signal (< 1 min) is a form of necrotic cell death. The second imaged neutrophil (NP2) had not entirely engulfed the bacterial aggregate it is associated with, and this neutrophil seemed to be undergoing a process called netosis (Cabrini et al., 2010; Francis et al., 2014). This cell showed a nuclear membrane that was not intact, and had granules at the plasma membrane releasing their content into the extracellular space in which a large aggregate of bacteria was located (Fig. 4D; Movie 10). In CLSM images, this cell was observed to be interacting with a large aggregate of *Mm* in the preceding 30 min, which had previously been contained by another neutrophil (Fig. 4C).

In the SBFSEM images we also observed *Mm*-infected epithelial cells in the process of undergoing extrusion (Fig. S4G). These cells did not show a fluorescent signal associated with macrophages or neutrophils in the CLSM images. Using 3D information provided by SBFSEM, we could observe that the bacterial aggregate was entirely contained within an epithelial cell. This presence of a bacterial aggregate inside an epithelial cell most likely results from bacterial uptake at the basal side of the cell (probably by efferocytosis), which subsequently underwent extrusion at the apical side of the epithelium.

DISCUSSION

In the present study, we show the specific key functions of macrophages and neutrophils during the dynamic early expansion process of a tissue-localized *Mm* infection in zebrafish larvae. In Fig. 5, a schematic overview of the cellular processes that were observed in this study during the different phases of early granuloma development is shown. The early granuloma development was observed to consist of three phases, the lag, exponential and stationary phase, which are characterized by distinct cellular processes.

The localized infection model used in this study enabled us to visualize the infection process in great detail, from the first infection of macrophages and neutrophils to the granuloma stage. Using this model we performed time-lapse CLSM, which was additionally combined with ultrastructure analysis using TEM or SBFSEM. Using other routes of infecting zebrafish embryos or larvae the function of macrophages in the stationary phase has been studied extensively (Lesley and Ramakrishnan, 2008; Davis and Ramakrishnan, 2009), but our model has additionally provided novel insights into specific key functions of macrophages and neutrophils during the lag and exponential phase of *Mm* infection in zebrafish larvae. The tail fin infection model complements other models, using different routes of infection in zebrafish larvae, by enabling the study of the initial processes in the infection process and could be considered as a model for *Mtb* infection. This model can be used to investigate the primary events of an infection caused by bacteria that have crossed the epithelial barrier, which is a well-known route for *Mtb* in the human lung.

The macrophages appear to play a specific role in the efferocytosis of both dead macrophages and neutrophils that were infected with *Mm*. Efferocytosis is a process to clear out apoptotic bodies and necrotic material (Erwig and Henson, 2008). During

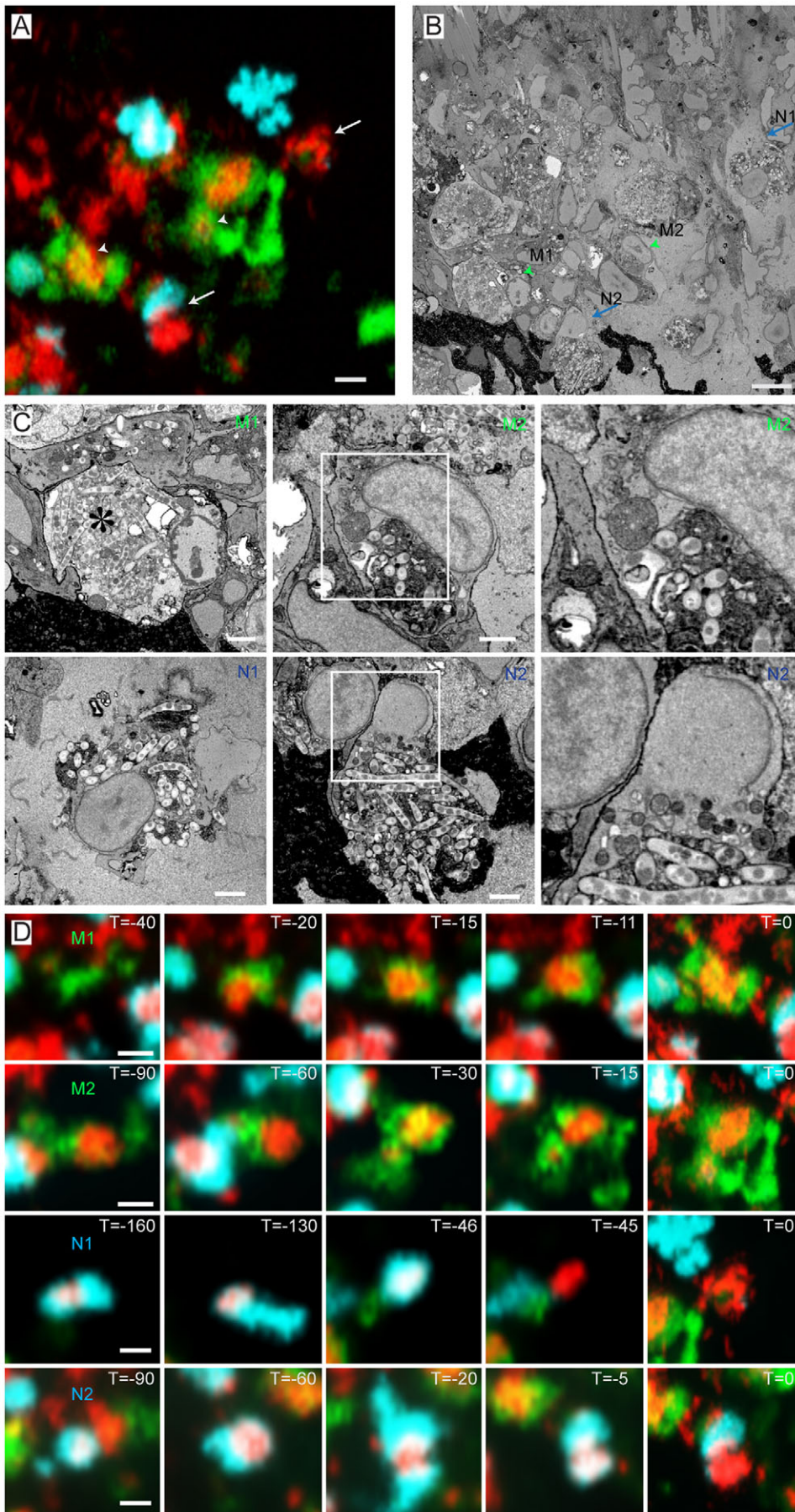


Fig. 4. Ultrastructure of correlated macrophages and neutrophils in 3D serial block-face SEM images. (A) High-resolution CLSM image of an infected tail fin after live-cell imaging and fixation. (B) SBFSEM image of the same region as in A showing correlated macrophages (arrowheads) and neutrophils (arrows). (C) Higher magnification SBFSEM images of the two macrophages and two neutrophils indicated in A and B. (D) Frames from time-lapse imaging showing the macrophages and neutrophils in C at previous time points. The macrophage (M1) with a fragmented nucleus contains a high *Mm* content, indicated by the asterisk in C. This macrophage phagocytized the bacterial content ~30 min before fixation. Macrophage M2 contains a large aggregate of *Mm* which was phagocytized *Mm* ~1.5 h before fixation. Neutrophil N1 shows a rapid signal disappearance ~45 min before the fixation (D). Neutrophil N2 was recruited to the bacterial aggregate ~30 min before fixation (D). Scale bars: 10 μ m (A–C); 2 μ m (D).

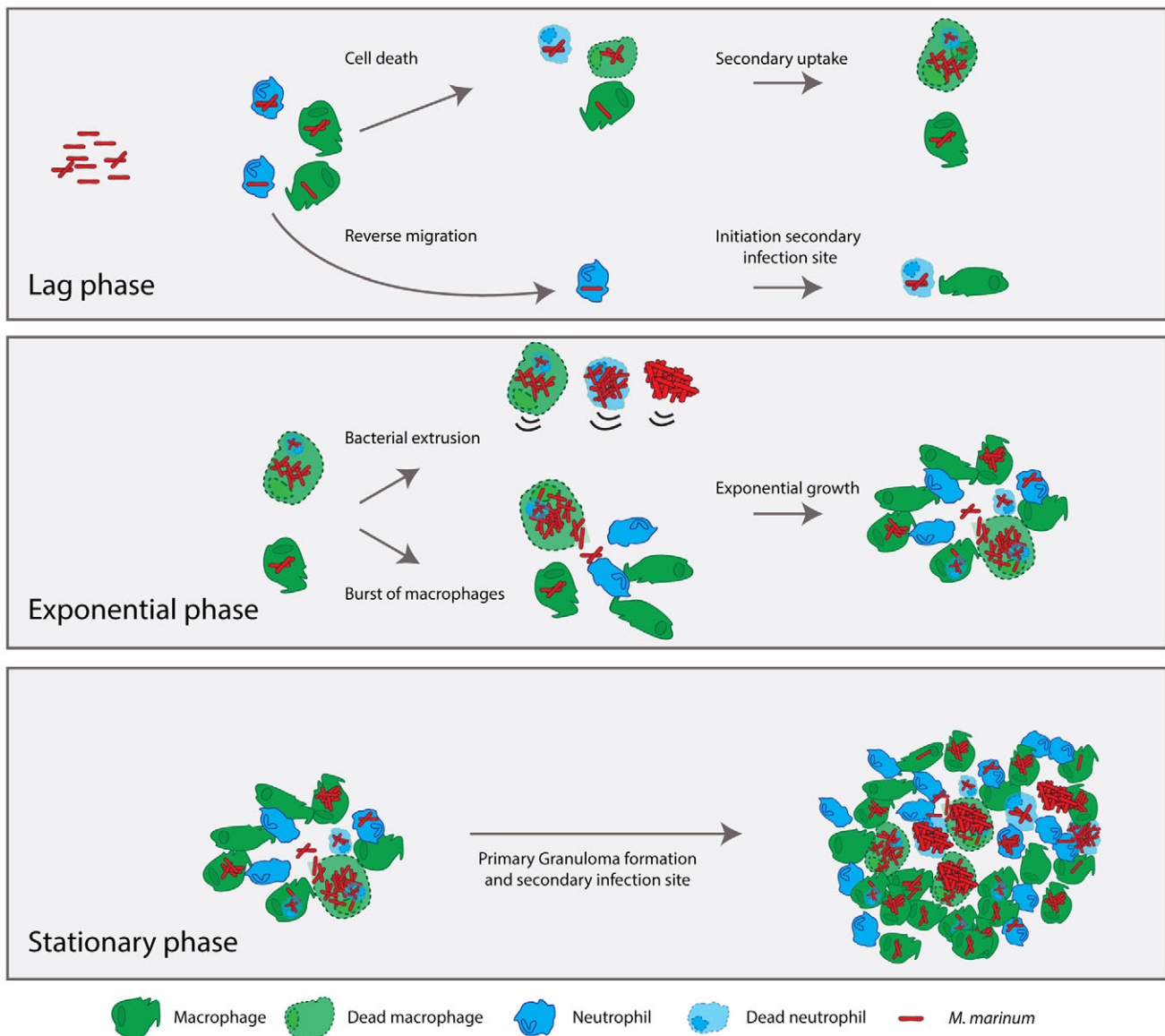


Fig. 5. Overview of *Mm* infection in the tail fin of zebrafish larvae. This schematic overview summarizes all processes taking place during the course of infection. At the lag phase, continuous cell death and efferocytosis by the macrophages leads to accumulation of *Mm* in a few macrophages at 12 hpi. Reverse migration was more frequently observed for infected neutrophils than for macrophages. The exponential phase is characterized by macrophage burst and bacterial extrusion. At the stationary phase, the granulomas increase in size and secondary granulomas are observed.

wound healing and inflammatory responses, efferocytosis by macrophages and neutrophils is essential to remove dead cells from the tissue (Rydell-Törmänen et al., 2006). By following trajectories of numerous individual macrophages and neutrophils, as well as their bacterial load and lifespan, for up to 18 h, we were able to clearly confirm earlier observations on the role of macrophages in efferocytosis (Davis and Ramakrishnan, 2009). Additionally, our results demonstrate that neutrophils also carry out efferocytosis in ~15% of cases. Continuous efferocytosis by macrophages resulted in a high bacterial contents in these cells, leading to the burst of macrophages when they were unable to retain this large number of pathogens. Burst of macrophages containing high numbers of intracellular *Mtb* has been demonstrated to induce cell death and promote extracellular spread of infection (Lee et al., 2006).

Neutrophils were shown in our study to be efficient in phagocytosis of tissue-localized *Mm* and contribute largely to the dissemination of the bacteria. The role of macrophages in the

dissemination of mycobacterial infections has been studied extensively, but the role of neutrophils is less clear (Davis and Ramakrishnan, 2009). A study in a murine infection model using an attenuated *M. bovis* strain (BCG) suggested that infected neutrophils migrate through afferent lymphatics to lymphoid tissue and can spread the bacterial infection (Abadie et al., 2005). Although neutrophils were not observed to phagocytose *Mm* following injection of bacteria into the bloodstream or the hindbrain of zebrafish embryos, subcutaneous infection studies in zebrafish larvae have demonstrated phagocytosis of bacteria (including *E. coli* and *Mm*) by neutrophils, indicating a tissue-dependency for this process (Yang et al., 2012; Davis et al., 2002; Colucci-Guyon et al., 2011; Belon et al., 2014). Here, we show that neutrophils can efficiently phagocytose mycobacteria at the initial infection site, and undergo reverse migration more frequently than macrophages. Owing to their high mobility, neutrophils might contribute more to the dissemination of bacteria than macrophages.

Epithelium-mediated extrusion of the bacterial content after efferocytosis of infected leukocytes was observed by CLSM, TEM and SBFSEM, and was shown to contribute to bacterial clearance. Extrusion of dead or infected epithelial cells is important for the preservation of the epithelial barrier, and it is therefore suggested not to be limited to (myco)bacterial clearance (Gu and Rosenblatt, 2012; Eisenhoffer et al., 2012). Apical extrusion of *Salmonella*-infected epithelial cells into the lumen has been observed in the gall bladder of infected mice (Knodler et al., 2010). To our knowledge this process has not been shown yet for mycobacterium infection, and the role of extrusion by the lung epithelium is still unclear. In the case of *Mtb* infection, which primarily affects the lungs in humans, extrusion might represent an important mechanism in the clearance of *Mtb*. Alternatively, mycobacteria might exploit extrusion as a strategy for avoiding the pro-inflammatory response and the process might therefore facilitate dissemination from human to human.

By following the dynamics of the leukocytes during the course of infection, we show that many macrophages and neutrophils underwent cell death during the process of *Mm* infection. Although mycobacteria are notorious for their ability to block apoptosis (Lee et al., 2006; Repasy et al., 2013), our correlative light and electron microscopy images show that macrophages with a large bacterial content, most likely acquired by efferocytosis, have a fragmented nucleus. In addition, by using CLSM, clear fragmentation of infected macrophages, another characteristic of apoptotic cell death, was observed (Fig. 2G; Fig. S2A). Based on light microscopy observations, the rapid signal disappearance of uninfected neutrophils was previously suggested to be apoptosis (Renshaw et al., 2006). Our correlative imaging shows, however, that these cells are most likely in a process of undergoing necrosis. Necrotic cells might lose their fluorescence due to a rapid denaturation of the fluorescent proteins, as a result of the release of lysosomal content and abundant peroxides into the cytoplasm (Artal-Sanz et al., 2006). We also demonstrate that neutrophils are able to undergo netosis, which is often associated with necrosis (Cabrinì et al., 2010; Francis et al., 2014). In cell culture studies, it has been shown that neutrophils are able to sense microbe size and selectively release extracellular traps in response to large pathogens such as *Candida albicans* hyphae and extracellular aggregates of *Mycobacterium bovis* (Branzk et al., 2014).

In summary, our data show that neutrophils have different roles in the early progression of a tissue-localized mycobacterial infection. Our results show that neutrophils are able to phagocytose mycobacteria and contribute to their dissemination. Macrophages play a major role in efferocytosis, resulting in large bacterial aggregates that can cause burst of macrophages or extrusion out of the tissue. The data show a major role for macrophage burst that results in increased spreading of the pathogen. By contrast, the main host–pathogen interaction resulting in a decreased bacterial burden was observed to be bacterial extrusion.

MATERIALS AND METHODS

Zebrafish strains and maintenance

Zebrafish were handled in compliance with the local animal welfare regulations and maintained according to standard protocols (www.zfin.org). The ABTL wild-type zebrafish strain and the transgenic lines, *Tg(mpeg1:eGFP)gl22*, and *Tg(lyz:DsRed2)nz50* strains were used for this study. All fish were raised and grown at 28.5°C on a 14-h-light–10-h-dark cycle. Embryos were obtained from natural spawning at the beginning of the light period and kept in egg water (60 µg/ml Instant Ocean sea salts).

Injection condition

The *M. marinum* M strain fluorescently labeled with E2-crimson was used and prepared at ~500 cfu per 1 nl as previously described (Benard et al.,

2012). Borosilicate glass micro capillaries (Harvard Apparatus) were used with a micropipette puller device (Sutter Instruments Inc.) for preparing microinjection needles. Zebrafish larvae were injected in the tail fin at 3 dpf using the Femtojet microinjection system (Eppendorf) with a fine (~5 to 10 µm) needle tip broken off with tweezers and mounted at a 30° angle. Larvae were anesthetized in egg water with 200 µg/ml 3-aminobenzoic acid (tricaine; Sigma-Aldrich) and injected between the two epidermal layers at the ventral part of the tail fin (Fig. 1). Morpholino against interferon regulatory factor-8 (*irf8*) (Li et al., 2011) was injected into yolk at the one-cell stage. A standard control morpholino (Genetools) was used as a negative control.

Confocal laser scanning microscopy

Larvae were anesthetized with 200 µg/ml tricaine and mounted in 0.7% low-melting-point agarose (Sigma-Aldrich) and imaged with the Nikon A1 confocal laser scanning microscope using the 488-, 561- and 641-nm laser lines with a 20× objective (NA 0.75) in resonance mode. Images were analyzed using NIS-Elements analysis software (Nikon). The bacterial burden was analyzed on the max-projection images (12 bit). Binary areas were created based on the *M. marinum* fluorescent signal using a threshold above 900 for the larvae at 0 dpi to 2 dpi, and a threshold above 1700 for larvae from 3 dpi to 5 dpi. The number of macrophages and neutrophils and all mentioned events were counted manually. Tracks were generated using Nis elements and mismatched tracks were manually corrected. The macrophage and neutrophil interactions during infection of 225 individual larvae were imaged at ~60 s per frame for 18 h at 28.5°C. For the lag phase, 33 larvae were analyzed (*n*=70 macrophages and 57 neutrophils) between 6 and 18 h. Larvae that moved out of view in less than 6 h were removed from the analysis. For the exponential phase and stationary phase, 60 larvae and 40 larvae were analyzed, respectively. The clearly observable macrophage burst events were counted manually and the bacterial extrusion events were scored manually to a maximum of 10 events per larva based on bacterial content released from the tissue.

Transmission electron microscopy

Before being used for electron microscopy the zebrafish larvae were anesthetized with 200 µg/ml tricaine and fixated in 2% glutaraldehyde and 2% paraformaldehyde in sodium cacodylate buffer (pH 7.2) for 3 h at room temperature followed by fixation for 16 h at 4°C. Post-fixation was performed in 1% osmium tetroxide in sodium cacodylate buffer for 1 h at room temperature. After dehydration through a graded series of ethanol, all specimens were kept in epoxy resin (Agar Scientific) for 16 h before embedding. Ultrathin sections were collected on Formvar-coated one-hole copper grids (Agar Scientific) stained with 2% uranyl acetate in 50% ethanol and lead citrate for 10 min each. Electron microscopy images were obtained with a JEOL JEM-1010 transmission electron microscope (Tokyo, Japan) equipped with an Olympus Megaview camera (Tokyo, Japan).

Block-face scanning electron microscopy

The larvae were prepared using a protocol modified from Deerinck et al. (<http://gatan.actonservice.com/acton/attachment/11413/f-017e/1/-/-/-/sbfsem%20sample%20prep%20protocol.pdf>). Before being used for SBFSEM, the zebrafish larvae were anesthetized with 200 µg/ml tricaine, imaged alive by CLSM and afterwards immediately fixed in 0.5% glutaraldehyde and 2% paraformaldehyde in PHEM buffer (pH 6.9) for 2 h at room temperature followed by fixation in 2% glutaraldehyde and 2% paraformaldehyde in sodium cacodylate buffer (pH 7.2) for 16 h at 4°C. Postfixation was performed in a solution of 4% osmium tetroxide and 3% potassium ferrocyanide (1:1 ratio) in 0.3 M sodium cacodylate buffer (pH 7.2), 20 min in 1% ThioCarboHydrazide (TCH), followed by incubation for 30 min in 2% osmium tetroxide, 1 h in 1% uranyl acetate and 30 min in Waltons lead aspartate at 60°C. After dehydration through a graded series of ethanol, all specimens were kept in epoxy resin (Agar Scientific) for 16 h before embedding. Blocks were trimmed and glued on a cryopin and examined in a Quanta FEG 250 with a Gatan 3View Ultramicrotome module using the BSE mode to perform 3D block-face imaging by cutting 150-nm sections.

The data was segmented and aligned with CLSM images using Amira 3.5 (FEI) software.

Statistical analysis

All data were analyzed (Prism version 5.0, GraphPad Software) using Kruskal–Wallis one-way analysis of variance (ANOVA) with Dunnett's post-test for multiple groups and Mann–Whitney test for comparing two groups. Error bars represent mean±s.e.m. Statistical significance was assumed at $P<0.05$ and groups labeled with the same letter do not differ significantly.

Acknowledgements

We thank Tobias Starborg (University of Manchester) for technical assistance and Bram Koster (LUMC) for helpful discussion.

Competing interests

The authors declare no competing or financial interests.

Author contributions

Conceptualization, R.H., A.H.M., H.P.S. and M.J.M.S.; methodology, R.H. and G.E.M.L.; formal analysis, R.H.; investigation, R.H., G.E.M.L. and H.M.S.; writing original draft, R.H. and M.J.M.S.; writing, review and editing, M.J.M.S., A.H.M. and H.P.S.; supervision, M.J.M.S. and H.P.S.; funding acquisition, H.P.S.

Funding

Infectious disease research in our laboratory is supported by the European Union Seventh Framework Programme project ZF-HEALTH [grant number HEALTH-F4-2010-242048] and the Cytron II Program [LSH framework number FES0908].

Data availability

The movies associated with this paper are deposited at dryad: <http://dx.doi.org/10.5061/dryad.08803>

Supplementary information

Supplementary information available online at <http://jcs.biologists.org/lookup/doi/10.1242/jcs.135194.supplemental>

References

- Abadie, V., Badell, E., Douillard, P., Ensergueix, D., Leenen, P. J. M., Tanguy, M., Fiette, L., Saeland, S., Gicquel, B. and Winter, N. (2005). Neutrophils rapidly migrate via lymphatics after *Mycobacterium bovis* BCG intradermal vaccination and shuttle live bacilli to the draining lymph nodes. *Blood* **106**, 1843–1850.
- Armstrong, J. A. and Hart, P. D. (1971). Response of cultured macrophages to *Mycobacterium tuberculosis*, with observations on fusion of lysosomes with phagosomes. *J. Exp. Med.* **134**, 713.
- Artal-Sanz, M., Samara, C., Syntichaki, P. and Tavernarakis, N. (2006). Lysosomal biogenesis and function is critical for necrotic cell death in *Caenorhabditis elegans*. *J. Cell Biol.* **173**, 231–239.
- Baxt, L. A., Garza-Mayers, A. C. and Goldberg, M. B. (2013). Bacterial subversion of host innate immune pathways. *Science* **340**, 697–701.
- Belon, C., Gannoun-Zaki, L., Lutfalla, G., Kremer, L. and Blanc-Potard, A.-B. (2014). *Mycobacterium marinum* MgtC plays a role in phagocytosis but is dispensable for intracellular multiplication. *PLoS ONE* **9**, e116052.
- Benard, E. L., van der Sar, A. M., Ellett, F., Lieschke, G. J., Spaik, H. P. and Meijer, A. H. (2012). Infection of zebrafish embryos with intracellular bacterial pathogens. *J. Vis. Exp.* **61**, doi:10.3791/3781.
- Berry, M. P. R., Graham, C. M., McNab, F. W., Xu, Z., Bloch, S. A. A., Oni, T., Wilkinson, K. A., Banchereau, R., Skinner, J., Wilkinson, R. J. et al. (2010). An interferon-inducible neutrophil-driven blood transcriptional signature in human tuberculosis. *Nature* **466**, 973–977.
- Branzk, N., Lubojemska, A., Hardison, S. E., Wang, Q., Gutierrez, M. G., Brown, G. D. and Papayannopoulos, V. (2014). Neutrophils sense microbe size and selectively release neutrophil extracellular traps in response to large pathogens. *Nature* **15**, 1017–1025.
- Cabrini, M., Nahmod, K. and Geffner, J. (2010). New insights into the mechanisms controlling neutrophil survival. *Curr. Opin. Hematol.* **17**, 31–35.
- Cambier, C. J., Takaki, K. K., Larson, R. P., Hernandez, R. E., Tobin, D. M., Urdahl, K. B., Cosma, C. L. and Ramakrishnan, L. (2014). *Mycobacteria* manipulate macrophage recruitment through coordinated use of membrane lipids. *Nature* **505**, 218–222.
- Colucci-Guyon, E., Tinevez, J.-Y., Renshaw, S. A. and Herbomel, P. (2011). Strategies of professional phagocytes in vivo: unlike macrophages, neutrophils engulf only surface-associated microbes. *J. Cell Sci.* **124**, 3053–3059.
- Davis, J. M. and Ramakrishnan, L. (2009). The role of the granuloma in expansion and dissemination of early tuberculous infection. *Cell* **136**, 37–49.
- Davis, J. M., Clay, H., Lewis, J. L., Ghori, N., Herbomel, P. and Ramakrishnan, L. (2002). Real-time visualization of mycobacterium-macrophage interactions leading to initiation of granuloma formation in zebrafish embryos. *Immunity* **17**, 693–702.
- Denk, W. and Horstmann, H. (2004). Serial block-face scanning electron microscopy to reconstruct three-dimensional tissue nanostructure. *PLoS Biol.* **2**, e329.
- Eisenhoffer, G. T., Loftus, P. D., Yoshigi, M., Otsuna, H., Chien, C.-B., Morcos, P. A. and Rosenblatt, J. (2012). Crowding induces live cell extrusion to maintain homeostatic cell numbers in epithelia. *Nature* **484**, 546–549.
- Elks, P. M., Brizee, S., van der Vaart, M., Walmsley, S. R., van Eeden, F. J., Renshaw, S. A. and Meijer, A. H. (2013). Hypoxia inducible factor signaling modulates susceptibility to mycobacterial infection via a nitric oxide dependent mechanism. *PLoS Pathog.* **9**, e1003789.
- Ellett, F., Pase, L., Hayman, J. W., Andrianopoulos, A. and Lieschke, G. J. (2011). mpeg1 promoter transgenes direct macrophage-lineage expression in zebrafish. *Blood* **117**, e49–e56.
- Erwig, L.-P. and Henson, P. M. (2008). Clearance of apoptotic cells by phagocytes. *Cell Death Differ.* **15**, 243–250.
- Eum, S.-Y., Kong, J.-H., Hong, M.-S., Lee, Y.-J., Kim, J.-H., Hwang, S.-H., Cho, S.-N., Via, L. E. and Barry, C. E. (2010). Neutrophils are the predominant infected phagocytic cells in the airways of patients with active pulmonary TB. *Chest* **137**, 122–128.
- Fink, S. L. and Cookson, B. T. (2005). Apoptosis, pyroptosis, and necrosis: mechanistic description of dead and dying eukaryotic cells. *Infect. Immun.* **73**, 1907–1916.
- Francis, R. J., Butler, R. E. and Stewart, G. R. (2014). *Mycobacterium tuberculosis* ESAT-6 is a leukocidin causing Ca²⁺ influx, necrosis and neutrophil extracellular trap formation. *Cell Death Dis.* **5**, e1474.
- Gu, Y. and Rosenblatt, J. (2012). New emerging roles for epithelial cell extrusion. *Curr. Opin. Cell Biol.* **24**, 865–870.
- Hall, C., Flores, M. V., Storm, T., Crosier, K. and Crosier, P. (2007). The zebrafish lysozyme C promoter drives myeloid-specific expression in transgenic fish. *BMC Dev. Biol.* **7**, 42.
- Hosseini, R., Lamers, G. E. M., Hodzic, Z., Meijer, A. H., Schaaf, M. J. and Spaik, H. P. (2014). Correlative light and electron microscopy imaging of autophagy in a zebrafish infection model. *Autophagy* **10**, 1844–1857.
- Hosseini, R., Lamers, G. E. M., Soltani, H. M., Meijer, A. H., Spaik, H. P. and Schaaf, M. J. M. (2016). Data from: Efferocytosis and extrusion of leukocytes determine the progression of early mycobacterial pathogenesis. *Dryad Digital Repository*. <http://dx.doi.org/10.5061/dryad.08803>.
- Houben, E. N. G., Korotkov, K. V. and Bitter, W. (2013). Take five - Type VII secretion systems of *Mycobacteria*. *Biochim. Biophys. Acta* **1843**, 1707–1716.
- Kimmel, C. B., Ballard, W. W., Kimmel, S. R., Ullmann, B. and Schilling, T. F. (1995). Stages of embryonic development of the zebrafish. *Dev. Dyn.* **203**, 253–310.
- Knodler, L. A., Vallance, B. A., Celli, J., Winfree, S., Hansen, B., Montero, M. and Steele-Mortimer, O. (2010). Dissemination of invasive *Salmonella* via bacterial-induced extrusion of mucosal epithelia. *Proc. Natl. Acad. Sci. USA* **107**, 17733–17738.
- Lee, J., Remold, H. G., Jeong, M. H. and Kornfeld, H. (2006). Macrophage apoptosis in response to high intracellular burden of *Mycobacterium tuberculosis* is mediated by a novel caspase-independent pathway. *J. Immunol.* **176**, 4267–4274.
- Lesley, R. and Ramakrishnan, L. (2008). Insights into early mycobacterial pathogenesis from the zebrafish. *Curr. Opin. Microbiol.* **11**, 277–283.
- Li, L., Jin, H., Xu, J., Shi, Y. and Wen, Z. (2011). Irf8 regulates macrophage versus neutrophil fate during zebrafish primitive myelopoiesis. *Blood* **117**, 1359–1369.
- Lowe, D. M., Redford, P. S., Wilkinson, R. J., O'Garra, A. and Martineau, A. R. (2012). Neutrophils in tuberculosis: friend or foe? *Trends Immunol.* **33**, 14–25.
- MacMicking, J. D. (2012). Interferon-inducible effector mechanisms in cell-autonomous immunity. *Nat. Rev. Immunol.* **12**, 367–382.
- Martin, C. J., Peters, K. N. and Behar, S. M. (2013). Macrophages clean up: efferocytosis and microbial control. *Curr. Opin. Microbiol.* **17**, 17–23.
- Meijer, A. H., van der Sar, A. M., Cunha, C., Lamers, G. E. M., Laplante, M. A., Kikuta, H., Bitter, W., Becker, T. S. and Spaik, H. P. (2007). Identification and real-time imaging of a myc-expressing neutrophil population involved in inflammation and mycobacterial granuloma formation in zebrafish. *Dev. Comp. Immunol.* **32**, 36–49.
- Nouailles, G., Dorhoi, A., Koch, M., Zerrahn, J., Weiner, J., Faé, K. C., Arrey, F., Kuhlmann, S., Bandermann, S., Loewe, D. et al. (2014). CXCL5-secreting pulmonary epithelial cells drive destructive neutrophilic inflammation in tuberculosis. *J. Clin. Invest.* **124**, 1268–1282.
- Peddie, C. J. and Collinson, L. M. (2014). Exploring the third dimension: volume electron microscopy comes of age. *Micron* **61**, 9–19.
- Renshaw, S. A., Loynes, C. A., Trushell, D. M. I., Elworthy, S., Ingham, P. W. and Whyte, M. K. B. (2006). A transgenic zebrafish model of neutrophilic inflammation. *Blood* **108**, 3976–3978.
- Renshaw, S. A. and Trede, N. S. (2012). A model 450 million years in the making: zebrafish and vertebrate immunity. *Dis. Model. Mech.* **5**, 38–47.

- Repasy, T., Lee, J., Marino, S., Martinez, N., Kirschner, D. E., Hendricks, G., Baker, S., Wilson, A. A., Kotton, D. N. and Kornfeld, H. (2013). Intracellular bacillary burden reflects a burst size for *Mycobacterium tuberculosis* in vivo. *PLoS Pathog.* **9**, e1003190.
- Rydell-Törmänen, K., Uller, L. and Erjefält, J. S. (2006). Neutrophil cannibalism – a back up when the macrophage clearance system is insufficient. *Respir. Res.* **7**, 143.
- Simeone, R., Bottai, D., Frigui, W., Majlessi, L. and Brosch, R. (2015). ESX/type VII secretion systems of mycobacteria: Insights into evolution, pathogenicity and protection. *Tuberculosis (Edinb.)* **95** Suppl 1, S150-S154.
- Silva, M. T., Silva, M. N. and Appelberg, R. (1989). Neutrophil-macrophage cooperation in the host defence against mycobacterial infections. *Microb. Pathog.* **6**, 369-380.
- Srivastava, S., Ernst, J. D. and Desvignes, L. (2014). Beyond macrophages: the diversity of mononuclear cells in tuberculosis. *Immunol. Rev.* **262**, 179-192.
- Swaim, L. E., Connolly, L. E., Volkman, H. E., Humbert, O., Born, D. E. and Ramakrishnan, L. (2006). *Mycobacterium marinum* infection of adult zebrafish causes caseating granulomatous tuberculosis and is moderated by adaptive immunity. *Infect. Immun.* **74**, 6108-6117.
- Tan, S. and Russell, D. G. (2015). Trans-species communication in the *Mycobacterium tuberculosis*-infected macrophage. *Immunol. Rev.* **264**, 233-248.
- Tobin, D. M., Vary, J. C., Ray, J. P., Walsh, G. S., Dunstan, S. J., Bang, N. D., Hagge, D. A., Khadge, S., King, M.-C., Hawn, T. R. et al. (2010). The *Ita4h* locus modulates susceptibility to mycobacterial infection in zebrafish and humans. *Cell* **140**, 717-730.
- Torraca, V., Masud, S., Spaink, H. P. and Meijer, A. H. (2014). Macrophage-pathogen interactions in infectious diseases: new therapeutic insights from the zebrafish host model. *Dis. Model. Mech.* **7**, 785-797.
- van der Vaart, M., Korbee, C. J., Lamers, G. E. M., Tengeler, A. C., Hosseini, R., Haks, M. C., Ottenhoff, T. H. M., Spaink, H. P. and Meijer, A. H. (2014). The DNA damage-regulated autophagy modulator DRAM1 links mycobacterial recognition via TLR-MYD88 to autophagic defense. *Cell Host Microbe* **15**, 753-767.
- van der Wel, N., Hava, D., Houben, D., Fluitsma, D., van Zon, M., Pierson, J., Brenner, M. and Peters, P. J. (2007). *M. tuberculosis* and *M. leprae* translocate from the phagolysosome to the cytosol in myeloid cells. *Cell* **129**, 1287-1298.
- Weiss, G. and Schaible, U. E. (2015). Macrophage defense mechanisms against intracellular bacteria. *Immunol. Rev.* **264**, 182-203.
- Yang, C.-T., Cambier, C. J., Davis, J. M., Hall, C. J., Crosier, P. S. and Ramakrishnan, L. (2012). Neutrophils exert protection in the early tuberculous granuloma by oxidative killing of mycobacteria phagocytosed from infected macrophages. *Cell Host Microbe* **12**, 301-312.